RSC Advances

PAPER

View Article Online
View Journal | View Issue

Check for updates

Cite this: *RSC Adv.*, 2019, **9**, 23071

PHB/PCL fibrous membranes modified with SiO_2@TiO_2-based core@shell composite nanoparticles for hydrophobic and antibacterial applications

Xinghuan Lin,[a] Shanshan Li,[a] Joonhoo Jung,[b] Wei Ma,[a] Lin Li,[a] Xuehong Ren,*[a] Yuyu Sun[b] and Tung-Shi Huang[c]

In order to prepare multifunctional fibrous membranes with hydrophobicity, antibacterial properties and UV resistance, we used silica and titanium dioxide for preparing SiO_2@TiO_2 nanoparticles (SiO_2@TiO_2 NPs) to create roughness on the fibrous membranes surfaces. The introduction of TiO_2 was used for improving UV resistance. N-Halamine precursor and silane precursor were introduced to modify SiO_2@TiO_2 NPs to synthesize SiO_2@TiO_2-based core@shell composite nanoparticles. The hydrophobic antibacterial fibrous membranes were prepared by a dip-pad process of electrospun biodegradable polyhydroxybutyrate/poly-ε-caprolactone (PHB/PCL) with the synthesized SiO_2@TiO_2-based core@shell composite nanoparticles. TEM, SEM and FT-IR were used to characterize the synthesized SiO_2@TiO_2-based core@shell composite nanoparticles and the hydrophobic antibacterial fibrous membranes. The fibrous membranes not only showed excellent hydrophobicity with an average water contact angle of 144° ± 1°, but also appreciable air permeability. The chlorinated fibrous membranes could inactivate all *S. aureus* and *E. coli* O157:H7 after 5 min and 60 min of contact, respectively. In addition, the chlorinated fibrous membranes exhibited outstanding cell compatibility with 102.1% of cell viability. Therefore, the prepared hydrophobic antibacterial degradable fibrous membranes may have great potential application for packaging materials.

Received 14th June 2019
Accepted 14th July 2019

DOI: 10.1039/c9ra04465e

rsc.li/rsc-advances

Open Access Article. Published on 25 July 2019. Downloaded on 1/9/2025 2:40:26 AM.
This article is licensed under a Creative Commons Attribution-NonCommercial 3.0 Unported Licence.

1 Introduction

Due to a heightened awareness of environmental issues, there is an increasing demand on biodegradable materials as potential replacements of traditional polymeric materials, such as polypropylene (PP), polyethylene (PE), and polystyrene (PS), to reduce waste accumulation.[1–3] Furthermore, there is a growing demand for global healthcare issues in regard to microbial infections in a variety of areas such as food packing, medical devices, textile materials and biomedical materials.[4–6] Therefore, the development of environmental-friendly alternative materials with efficient antibacterial properties is highly desirable.

Due to their biodegradability and biocompatibility, biodegradable materials have been widely investigated concerning potential applications as food packaging and biomedical materials.[7–9] However, the properties of the biodegradable materials for food packing and medical materials still show shortcomings, especially in respect to antibacterial properties. Therefore, there is an urgent need to impart antimicrobial performance to improve their range of uses. Recently, antimicrobial agents, such as inorganic metals and their oxides, organic macromolecules, including chitosan compounds and quaternary ammonium compounds, and N-halamine have been widely used.[10–17] Among these, N-halamine materials have extensively drawn attention due to their excellent antibacterial efficacies, broad-spectrum sterilization and easy regenerability.[18,19] Aside from antibacterial properties, high hydrophobicity of material surfaces is one of the most important characteristics for packaging materials. On one hand, materials applied for food packaging with excellent hydrophobicity can block the ingress of moisture and oxygen to slow down bacterial growth and food spoilage.[20] On the other hand, materials with prominent hydrophobicity can exhibit a self-cleaning function and may improve their antimicrobial properties. At present, a salient hydrophobic surface is mainly prepared by building a nano-structured surface and reducing surface energy on the substrate.[21]

Nanomaterial due to its small size and large specific surface area has many physical and chemical properties.[22–24]

[a]Key Laboratory of Eco-textiles of Ministry of Education, College of Textiles and Clothing, Jiangnan University, Wuxi, Jiangsu, 214122, China
[b]Department of Chemistry, University of Massachusetts Lowell, Lowell, 01854, USA
[c]Department of Poultry Science, Auburn 36849, AL, USA. E-mail: xhren@jiangnan.edu.cn

Open Access Article. Published on 25 July 2019. Downloaded on 1/9/2025 2:40:26 AM. This article is licensed under a Creative Commons Attribution-NonCommercial 3.0 Unported Licence.

Electrospinning is a well-known and cost-effective technique to produce nanofibers from various polymers. The resulting electrospun nanofibers are useful in many applications such as biomedical, filter and energy related materials.[25–27]

Over the last few years, nanoparticles including inorganic particles, metal particles and others have been synthesized to prepare different shapes and sizes with outstanding properties.[28,29] Subsequently, core@shell nanoparticles have attracted considerable attention for nanotechnology fields owing to chemical and colloidal stabilities, adjustable physical properties and controllability of interparticle interactions within assemblies.[30,31]

In our previous study,[32,33] we found that synthesized N-halamine siloxane compounds had poor stability under UV irradiation, because its Si-alkyl group bond easily decomposed which in return led to decreased chlorine content. Therefore, in this study, we used TiO_2 and SiO_2 for building SiO_2@TiO_2 NPs, which SiO_2 acted as a core for it is chemically inert, does not affect redox reactions at the core surface and can easily be modified with many other compounds,[34] while TiO_2 as a UV light protecting agent acted as the shell owing to its unique physical properties under UV light irradiation.[16,35] To improve the hydrophobicity, we grafted the N-halamine precursors and silane precursors onto the SiO_2@TiO_2 NPs to build multilevel nanostructures. Polyhydroxybutyrate/poly-ε-caprolactone (PHB/PCL) served as a biodegradable substrate that could be electrospun into nanofibers. Subsequently, the synthesized N-halamine containing SiO_2@TiO_2-based core@shell composite nanoparticles were deposited onto these fibrous membranes and chlorinated. Results demonstrated that the obtained membranes exhibited remarkable antimicrobial activity against *S. aureus* and *E. coli* O157:H7, respectively, outstanding hydrophobicity and appreciable air permeability. Moreover, the chlorinated fibrous membranes displayed excellent UVA light and storage stability. Besides, the active chlorine of that chlorinated fibrous membranes could easily be recovered.

2 Results and discussion

2.1 Characterization of SiO_2@TiO_2-based core@shell composite nanoparticles

The surface morphologies and structures of the nanoparticles were observed by TEM and FT-IR and the results are shown in Fig. 1. It can be seen that the size of the prepared SiO_2 NPs (Fig. 1A) was relatively uniform; the average diameter was determined to be 129.6 ± 10 nm, while the average diameter of SiO_2@TiO_2 NPs (Fig. 1B) was 274.5 ± 16 nm. It could be inferred that the thickness of shell (TiO_2) was 60 ± 5 nm. Upon modification with HDTMS and SPH, the size of SiO_2@TiO_2-based core@shell composite nanoparticles (Fig. 1C) was not visibly changed, which might due to the fact that HDTMS and SPH are rather small compounds compared to SiO_2@TiO_2 NPs.

FT-IR spectra (Fig. 1D) show the bands at around 1058, 945 and 794 cm^{-1} owing to asymmetric stretching vibration of Si–O–Si, stretching vibration of Si–O–H, and a symmetric stretching vibration of Si–O–Si, respectively.[36,37] The band at 1100 cm^{-1} in the spectra of SiO_2@TiO_2 NPs was assigned to the stretching vibration of Ti–O.[16] In contrast to SiO_2@TiO_2 NPs, SiO_2@TiO_2-based core@shell composite nanoparticles had a few new bands at 2915 and 2850 cm^{-1} attributed to the $-CH_3$ and $-CH_2-$ bending vibration of the HDTMS, while 1771 and 1712 cm^{-1} can be ascribed to the C=O stretching vibration of the SPH.[38]

2.2 Characterization of composite fibrous membranes

2.2.1 SEM. The surface morphology and diameters distribution of the fibrous membranes were observed by SEM and are shown in Fig. 2. The PHB/PCL fibrous membranes (Fig. 2A) obtained were bead-free; the fibrous diameter ranged from 0.5 μm to 4 μm with an average of 2.32 μm. It can be seen from Fig. 2B that the surface of the PHB/PCL–SiO_2@TiO_2–HDTMS/SPH membranes became rough and the average diameter of fibers was 2.49 μm, thus showed no significant difference compared with the PHB/PCL fibrous membranes. After chlorination (Fig. 2C), again there were no obvious changes in the surface morphologies and the average diameter of fibrous membranes measured 2.25 μm.

2.2.2 FT-IR. FT-IR spectra of the prepared fibrous membranes are shown in Fig. 3. Compared with the spectra of PHB/PCL fibrous membranes (a), additional bands appeared at 1771, 1084 and 794 cm^{-1} of PHB/PCL–SiO_2@TiO_2–HDTMS/SPH (b) which were assigned to the vibrational band of C=O, asymmetric stretching vibration of Si–O–Si and a symmetric stretching vibration of Si–O–Si on SiO_2@TiO_2-based core@shell composite nanoparticles, respectively.[36,37] Besides, the intensities of $-CH_3$ and $-CH_2-$ peak at 2918 and 2850 cm^{-1} in spectra (b) and (c) were obviously stronger than those in (a), which was mainly attributed to the long alkyl chains of HDTMS.[38] After chlorination, the characteristic vibrational band of C=O shifted from 1771 cm^{-1} to 1788 cm^{-1}, which was ascribed to the transformation of N–H bond to N–Cl bond.[39]

2.3 Thermal analysis

The TGA and DTG of fibrous membranes are shown in Fig. 4. There were two degradation steps that became apparent in the TGA curves for PHB/PCL fibrous membranes (Fig. 4A). PHB was the first to degrade with its weight loss temperature ranging from 250 to 300 °C.[26] And PCL was the second to degrade with its weight loss temperature ranging from 350 to 450 °C. The main decomposition temperature of PHB and PCL of PHB/PCL–SiO_2@TiO_2–HDTMS/SPH fibrous membranes was higher than these in curve of PHB/PCL fibrous membranes, which might be due to cross-linking of SiO_2@TiO_2 NPs at the surface of PHB/PCL fibrous membranes. There was a new degradation step of PHB/PCL–SiO_2@TiO_2–HDTMS/SPH fibrous membranes which was ascribed to SPH, and its weight loss occurred at 450 °C to 550 °C.[40] After chlorination, the main degradation temperature of PHB, PCL and SPH decreased. It is possible that the N–Cl bonds of SPH broke and further accelerated the thermal decomposition of fibrous membranes *via* a free radical process.[15] The remaining residual mass of PHB/PCL fibrous membranes was 1.17% at 600 °C, while it was 10.8% and 13.6% at 600 °C, respectively, before and after chlorination in case of PHB/PCL–SiO_2@TiO_2–HDTMS/SPH fibrous membranes. The

 This journal is © The Royal Society of Chemistry 2019

Open Access Article. Published on 25 July 2019. Downloaded on 1/9/2025 2:40:26 AM.
This article is licensed under a Creative Commons Attribution-NonCommercial 3.0 Unported Licence.

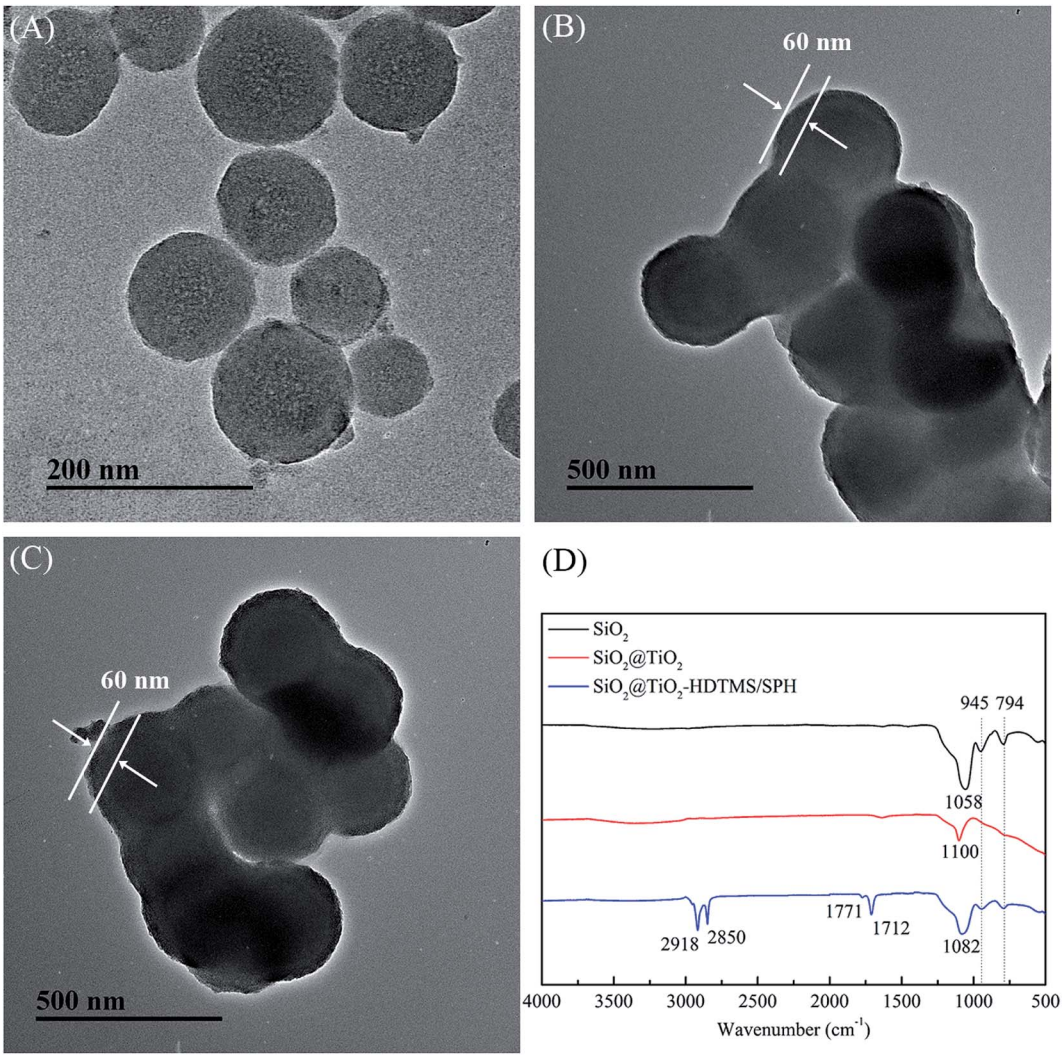

Fig. 1 TEM images of (A) SiO_2 NPs, (B) SiO_2@TiO_2 NPs and (C) SiO_2@TiO_2-based core@shell composite nanoparticles; (D) FT-IR spectra of nanoparticles.

final residual in case of PHB/PCL fibrous membranes at 600 °C was just carbon, while in case of PHB/PCL–SiO_2@TiO_2–HDTMS/SPH fibrous membranes at 600 °C it included nitrogen, silica and titanium.

2.4 Hydrophobicity and air permeability

The contact angles and air permeability of fibrous membranes were determined and the results are shown in Table 1. The surface of PHB/PCL fibrous membranes was quickly wetted with 2 μL of distilled water, while the surface of PHB/PCL–SiO_2@-TiO_2–HDTMS/SPH fibrous membranes exhibited outstanding hydrophobicity with a contact angle up to 144° ± 1°. There were no significant differences in contact angle before and after chlorination. The PHB/PCL fibrous membranes displayed excellent air permeability (54.6 ± 2.6 mm s^{-1}), whereas the air permeability of the PHB/PCL–SiO_2@TiO_2–HDTMS/SPH fibrous membranes declined to 44.8 ± 1.3 mm s^{-1}. After chlorination, the PHB/PCL–SiO_2@TiO_2–HDTMS/SPH fibrous membranes showed good air permeability of 50.9 ± 1.7 mm s^{-1}. Thus, the improvement in hydrophobicity of PHB/PCL fibrous membranes did not compromise the air permeability of the membranes after surface modified. In addition, the chlorination process made no difference to hydrophobicity and air permeability. Therefore, in conclusion the fibrous membranes had good hydrophobicity and air permeability and may have a great potential for applications as textile and biomedical materials.

2.5 Antibacterial efficacy

The antibacterial efficacy of fibrous membranes against *S. aureus* and *E. coli* O157:H7 were tested and the results are displayed in Fig. 5. The initial populations of *S. aureus* and *E. coli* O157:H7 were 1.03 × 10^6 CFU per sample and 1.00 × 10^6 CFU per sample. Clearly, the PHB/PCL fibrous membranes (Fig. 5A) had poor antibacterial property against *S. aureus* with log value of 0.011 (2.43%) reduction within 60 min. Similarly, the PHB/PCL fibrous membranes (Fig. 5B) only caused 0.145 log reduction of *E. coli* O157:H7 within 60 min. After modified with

Open Access Article. Published on 25 July 2019. Downloaded on 1/9/2025 2:40:26 AM.
This article is licensed under a Creative Commons Attribution-NonCommercial 3.0 Unported Licence.

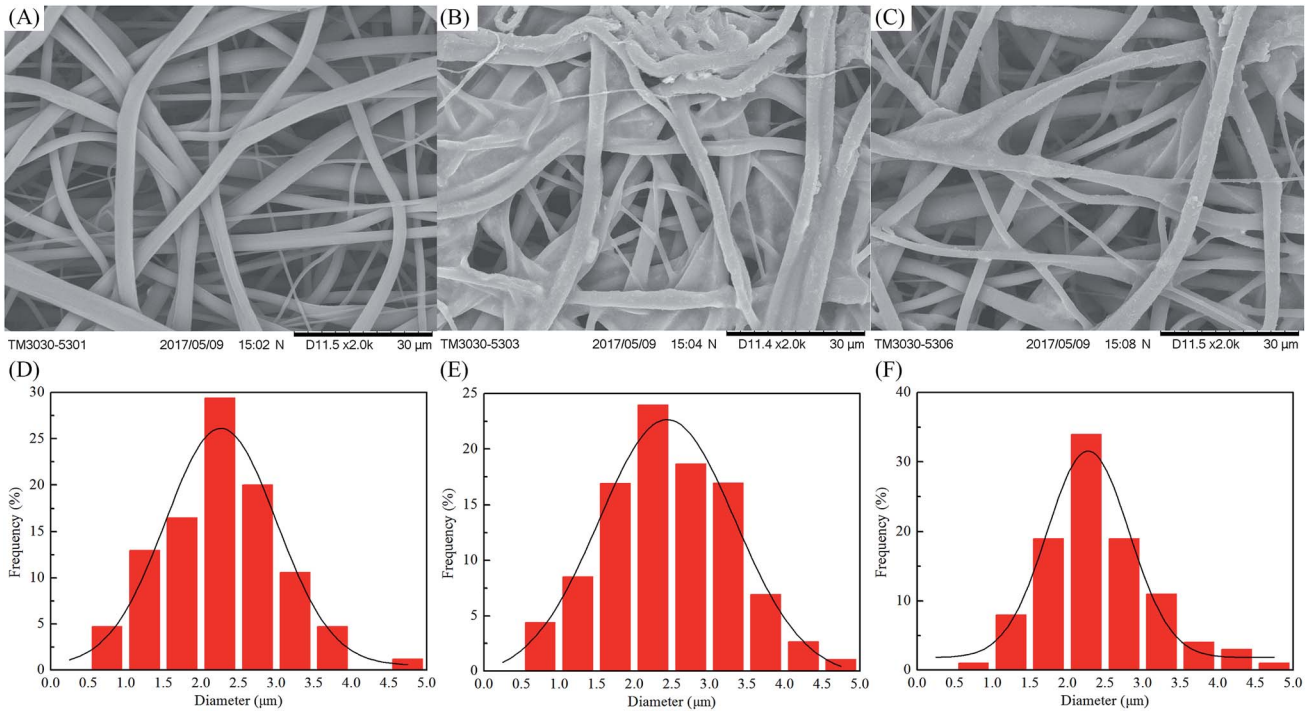

Fig. 2 SEM images and diameters distribution of PHB/PCL (A and D), PHB/PCL–SiO_2@TiO_2–HDTMS/SPH (B and E) and PHB/PCL–SiO_2@TiO_2–HDTMS/SPH–Cl (C and F) fibrous membranes.

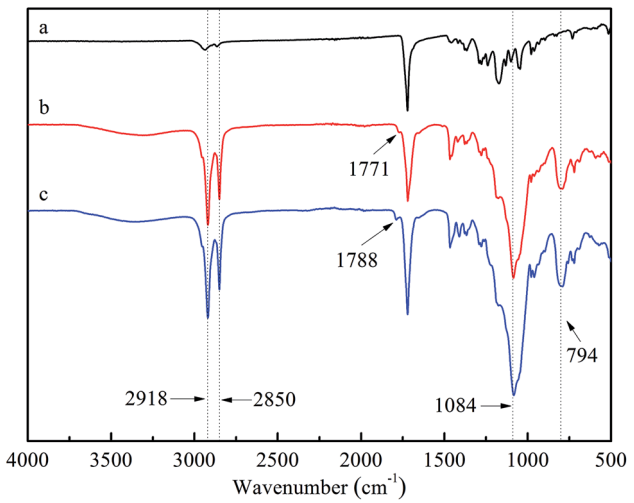

Fig. 3 FT-IR spectra of PHB/PCL (a), PHB/PCL–SiO_2@TiO_2–HDTMS/SPH (b) and PHB/PCL–SiO_2@TiO_2–HDTMS/SPH–Cl (c) fibrous membranes.

SiO_2@TiO_2-based core@shell composite nanoparticles, the bactericidal efficacies of fibrous membranes against *S. aureus* and *E. coli* O157:H7 improved slightly with log reductions of 0.111 and 0.210, respectively, which might be attributed to the addition of TiO_2.[35] In contrast, as expected, the bactericidal percentages of the chlorinated membranes against *S. aureus* and *E. coli* O157:H7 were dramatically increased with the extension of contact time. After chlorination, N–H bonds of SPH were converted to N–Cl bonds, which were able to release oxidative halogens (Cl^+) to attracted to bacterial organisms, and then destroyed the cell membrane of bacteria by oxidizing thiol groups or halogenating amino groups in proteins.[41] From Fig. 5A and B, it can be seen that the chlorinated fibrous membranes inactivated 100% of *S. aureus* and *E. coli* O157:H7 within 5 min and 60 min of contact time, respectively. The antibacterial efficiency of the chlorinated fibrous membranes against *S. aureus* was significantly higher than *E. coli* O157:H7. The different shapes and surface structures of bacteria might cause them to adhere to the samples at different degrees, which was in accordance with results reported by other research groups.[32,42,43]

2.6 Cytotoxicity test

The results of cytotoxicity tests of fibrous membranes were shown in Fig. 6. The cell viability cultured in extract solution of PHB/PCL fibrous membranes declined dramatically to 69.6% compared with the control sample. According to the International Standard Organization (ISO/EN 10993-5), the reduction of cell viability by more than 30% is considered a cytotoxic effect.[44] In this study, PHB/PCL fibrous membranes showed some degree of cytotoxic effect after 24 h incubation. After modified with SiO_2@TiO_2-based core@shell composite nanoparticles, the fibrous membranes showed good cell compatibility with 95.3% of cell viability. After chlorination, the cell viability of PHB/PCL–SiO_2@TiO_2–HDTMS/SPH fibrous membranes increased to 102.1%, which was higher than that of the control. The result is consistent with the previous report that low concentration of oxidative chlorine on the surface after deoxidation transferred

 This journal is © The Royal Society of Chemistry 2019

Open Access Article. Published on 25 July 2019. Downloaded on 1/9/2025 2:40:26 AM.
This article is licensed under a Creative Commons Attribution-NonCommercial 3.0 Unported Licence.

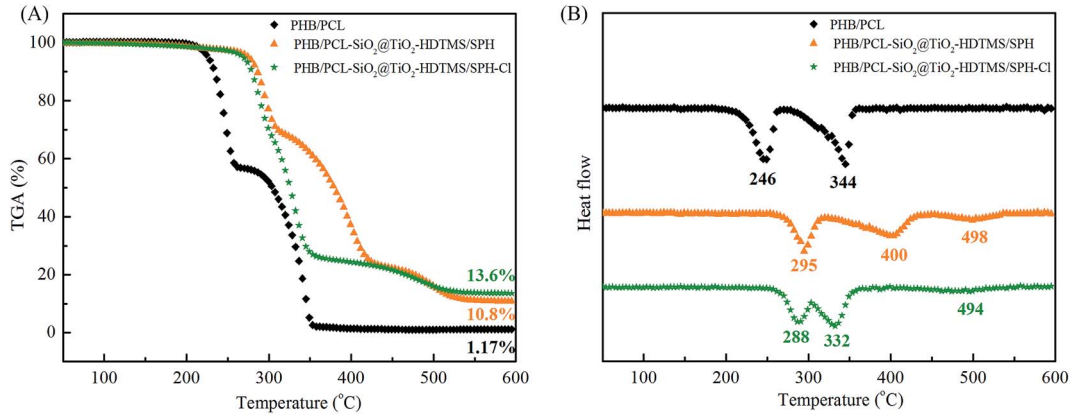

Fig. 4 TGA (A) and DTG (B) curves of the fibrous membranes.

into chloride containing Cl^- and these compounds could promote cell growth.[45]

2.7 UVA light stability and storage stability

The PHB/PCL–SiO_2@TiO_2–HDTMS/SPH–Cl fibrous membranes were evaluated for UVA light and storage stability, and the results are displayed in Fig. 7. From Fig. 7A, it can be seen that the active chlorine content decreased with the extension of irradiation time, and only 0.04 wt% (10.8% of the initial active chlorine content) of active chlorine content remained after 24 h exposure. The loss of active chlorine was attributed to the decomposition of N–Cl bonds.[46] After rechlorination, the active chlorine of the samples was 0.26 wt%, suggesting that 70% of the initial active chlorine content (Cl^+% = 0.37 wt%) could be regained. The unrecovered chlorine content was ascribed to decomposition of Si–C bond.[33,47] N-Halamine siloxane compound had poor UVA light stability because Si-alkyl group bond could break and result in the loss of the hydantoin ring under UV irradiation.[32,33] The introduction of TiO_2 in building the core@shell structure and further modification of the fibrous membranes could significantly increase UVA light stability. TiO_2 is composed of a full valence band and a vacant

Table 1 Hydrophobicity and air permeability of fibrous membranes

Samples (fibrous membranes)	Contact angle (°)	Air permeability (mm s^{-1})
PHB/PCL	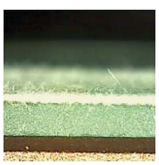 0	54.6 ± 2.6
PHB/PCL–SiO_2@TiO_2–HDTMS/SPH	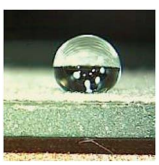 144 ± 1	44.8 ± 1.3
PHB/PCL–SiO_2@TiO_2–HDTMS/SPH–Cl	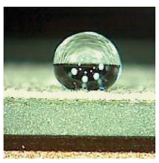 144 ± 2	50.9 ± 1.7

Open Access Article. Published on 25 July 2019. Downloaded on 1/9/2025 2:40:26 AM.
This article is licensed under a Creative Commons Attribution-NonCommercial 3.0 Unported Licence.

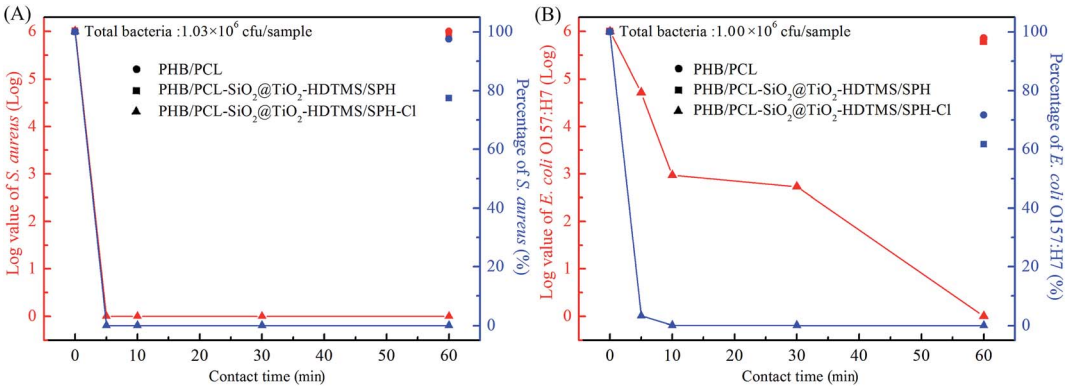

Fig. 5 Antibacterial efficacy of fibrous membranes against (A) *S. aureus* and (B) *E. coli* O157:H7.

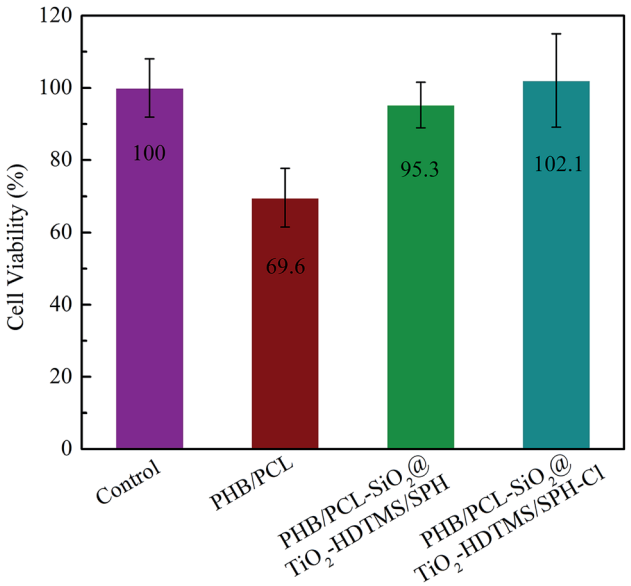

Fig. 6 Cell viability of rat skin fibroblasts on control and different fibrous membranes after 24 h incubation.

conduction band, which allows the electrons to become transitional between the valence band and the conduction band under UV light irradiation with wavelengths less than 387.5 nm.[16,35] Thus, TiO_2 played an important role as a UV light protecting agent to guard the structure of SPH from decomposition, improving the UVA light stability of the chlorinated fibrous membranes.

Fig. 7B shows that there was a slight decrease in the chlorine content over storage time when the samples were kept in the dark. After 60 days, the active chlorine content of the chlorinated PHB/PCL–SiO_2@TiO_2–HDTMS/SPH fibrous membranes was 0.30%, and thus 83.3% of the original chlorine content (0.37%), which still had efficient antibacterial effect.[48] After rechlorination, almost all of the active chlorine of the fibrous membranes was recovered. The above results indicated that the N–Cl bond of the chlorinated PHB/PCL–SiO_2@TiO_2–HDTMS/SPH fibrous membranes was relatively stable under dark condition. Overall, the good UVA light and storage stability as well as their chlorine rechargeability make the prepared antimicrobial fibrous membranes useful materials for numerous practical applications.

3 Experimental

3.1 Materials and characterization

Polyhydroxybutyrate (PHB, M_n = 30 000 g mol^{-1}) was provided by Tianjin Green Bio Materials Co., Ltd (Green Bio), China. 5,5-Dimethylhydantoin (DMH) was purchased from Hebei Yaguang

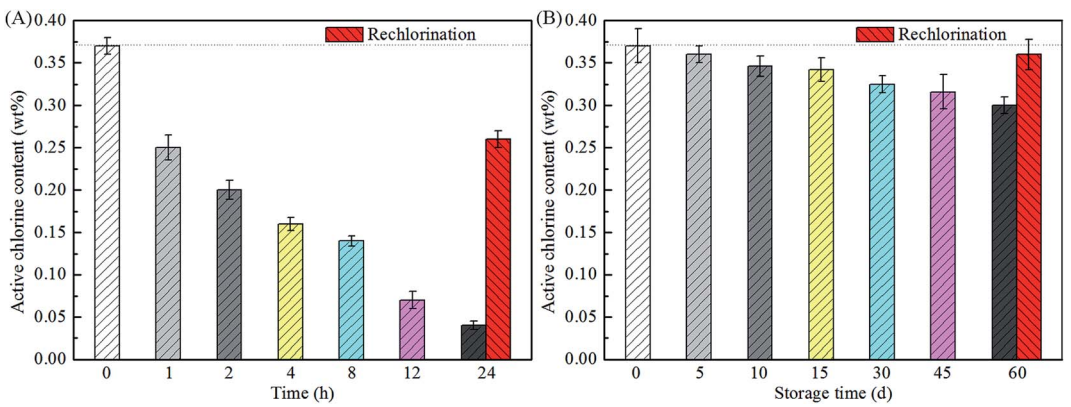

Fig. 7 UVA light stability (A) and storage stability (B) of chlorinated PHB/PCL–SiO_2@TiO_2–HDTMS/SPH fibrous membranes.

This journal is © The Royal Society of Chemistry 2019

Open Access Article. Published on 25 July 2019. Downloaded on 1/9/2025 2:40:26 AM.
This article is licensed under a Creative Commons Attribution-NonCommercial 3.0 Unported Licence.

Fine Chemical Co. Ltd. Octyl phenol ethoxylates-10 (OP-10) from Shengyu Chemical Co., Ltd, Shanghai, China. Poly-ε-caprolactone (PCL, M_n = 80 000 g mol^{-1}), tetra-*n*-butyl titanate (TBT), hexadecyltrimethoxysilane (HDTMS) and (3-chloropropyl) triethoxysilane were purchased from J&K Technology Co., Ltd, Shanghai, China. Tetraethoxysilane (TEOS), sodium hydroxide (NaOH), sodium thiosulfate ($Na_2S_2O_3$), sodium hypochlorite (10% chlorine content), azobis(isobutyronitrile) (AIBN), potassium iodide (KI), chloroform ($CHCl_3$), *N*,*N*-dimethylformamide (DMF), ethanol and acetic acid were purchased from Sinopharm Chemical Reagent Co., Ltd, Shanghai, China. Bacteria of *S. aureus* ATCC 6538 and *E. coli* O157:H7 ATCC 43895 (American Type Culture Collection, Rockville, MD) were used in this study.

The morphologies of membranes were characterized by scanning electron microscopy (TM3030, Hitachi High Technologies, Japan) and the average diameter and size distribution of fibers from the SEM images were determined by a nanomeasurer software (Department of Chemistry, Fudan University, Shanghai, China). Fourier transform infrared (FT-IR) spectra were tested by a NEXUS 470 spectrometer (Nicolet Instrument Corporation, USA). Transmission electron microscope (TEM) were characterized by a JEM 2100 TEM microscope operated at 200 kV (Hitachi High Technologies, Japan), and the samples (c = 0.1–0.2 g L^{-1}) were obtained by dipping copper 400-mesh carrier grids. Thermogravimetric analysis (TGA) was tested by a Q500 TGA (TA Instruments Co. Ltd., USA) *via* heating 5 mg sample from room temperature to 600 °C at a rate of 10 °C min. The air permeability was tested with a water vapor transmission tester (YG 461E, Ningbo Textile Instrument Co. Ltd., China).

3.2 Preparation of PHB/PCL electrospun fibrous membranes

Ten percent (w/v) of PHB/PCL (w/w, 40/60) were dissolved in chloroform at 45 °C for 3–5 h under stirring. The final solution was electrospun at room temperature to make fibrous membranes. And the parameters were as followed: 20 kV of voltage, 1.5 mL h^{-1} of flow rate and 20 cm of tip-to-collector distance.

3.3 Synthesis of 5,5-dimethyl-3-(3′-triethoxysilylpropyl) hydantoin (SPH)

5,5-Dimethyl-3-(3′-triethoxysilylpropyl)hydantoin (SPH) was synthesized according to S. D. Worley reported.[49] Hydantoin sodium salt was prepared by mixing DMH with an equimolar quantity of NaOH in ethanol to react for 10 min at 90 °C. After drying at 45 °C for 2 days, the prepared hydantoin sodium salt was dissolved in DMF, and subsequently (3-chloropropyl)triethoxysilane was added with stirring at 95 °C for 10 h. The SPH was obtained through filtration and evaporation of DMF.

3.4 Synthesis of SiO_2@TiO_2-based core@shell composite nanoparticles

Colloidal silica nanoparticles (SiO_2 NPs) were prepared according to the protocol of previous studies.[32] First, a mixture (100 mL) of ethanol, H_2O and 10% NH_4OH (v/v/v, 5 : 4 : 1) was stirred vigorously to form a homogeneous solution. Then, a stock solution containing 10 mL TEOS and 10 mL ethanol was added into the mixture at a rate of 0.5 mL min^{-1} with a constant pressure funnel. After mixing vigorously, the mixture solution was vigorously stirring at 60 °C for 2 h. Finally, the SiO_2 NPs were separated by centrifugation.

In the next step the SiO_2 NPs were dispersed uniformly in 100 mL ethanol : H_2O (19 : 1, v/v) in an ultrasonic bath for 30 min, and 0.5 g OP-10 was added into the mixture. Another solution containing 10 mL TTB and 10 mL ethanol was injected into the above mixture at a rate of 0.5 mL min^{-1} with a constant pressure funnel. The resulting mix was stirred vigorously at 50 °C for 12 h. Finally, the SiO_2@TiO_2 NPs were separated by centrifugation.

The prepared SiO_2@TiO_2 NPs were dispersed uniformly in the 100 mL ethanol solution and 0.5 g OP-10 was added to the dispersion in an ultrasonic bath for 30 min. Then, 8 wt% SPH, and 12 wt% HDTMS were added with vigorously stirring at room temperature for 4 h. The SiO_2@TiO_2-based core@shell composite nanoparticles were separated by centrifugation, washed 2 times with ethanol, and dried at 45 °C. In Scheme 1 the process is schematically illustrated.

3.5 Preparation of hydrophobic antibacterial fibrous membranes

Ten percent (w/v) of SiO_2@TiO_2-based core@shell composite nanoparticles and one percent (w/v) AIBN were dissolved in the ethanol solution in an ultrasonic bath for 30 min. The PHB/PCL fibrous membranes were dipped in the above colloidal solution, followed by two dips (30 s of each dip) and two pads (wet pick-up 75–80%). Then, the fibrous membranes were dried at 60 °C for 1 h. The treated fibrous membranes were washed thoroughly with ethanol and dried. And these membranes were called PHB/PCL–SiO_2@TiO_2–HDTMS/SPH. Then, fibrous membranes were soaked in a sodium hypochlorite solution (10 wt%, pH 7) at room temperature for 1 h to render antimicrobial properties. The chlorinated fibrous membranes were washed thoroughly and dried at 45 °C for 1 h to remove unbound chlorine. These membranes were called PHB/PCL–SiO_2@TiO_2–HDTMS/SPH–Cl.

3.6 Chlorine content measurement

The active chlorine content on fibrous membranes was tested by a modified iodometric/thiosulfate titration method. The active chlorine weight percent of fibrous membranes was calculated according to the eqn (1):

$$Cl^+(\%) = \frac{35.45 \times N \times V}{2 \times W} \times 100 \quad (1)$$

where, Cl^+ (%) is the weight percent of active chlorine on the membranes, N is the normality (equiv. per L) and V is the volume (L) of the $Na_2S_2O_3$ solution, respectively, while W is the weight (g) of chlorinated fibrous membranes.

3.7 Biocidal efficacy test

Gram-positive *S. aureus* (ATCC 6538) and Gram-negative *E. coli* O157:H7 (ATCC 43895) were used to test the antibacterial

Open Access Article. Published on 25 July 2019. Downloaded on 1/9/2025 2:40:26 AM.
This article is licensed under a Creative Commons Attribution-NonCommercial 3.0 Unported Licence.

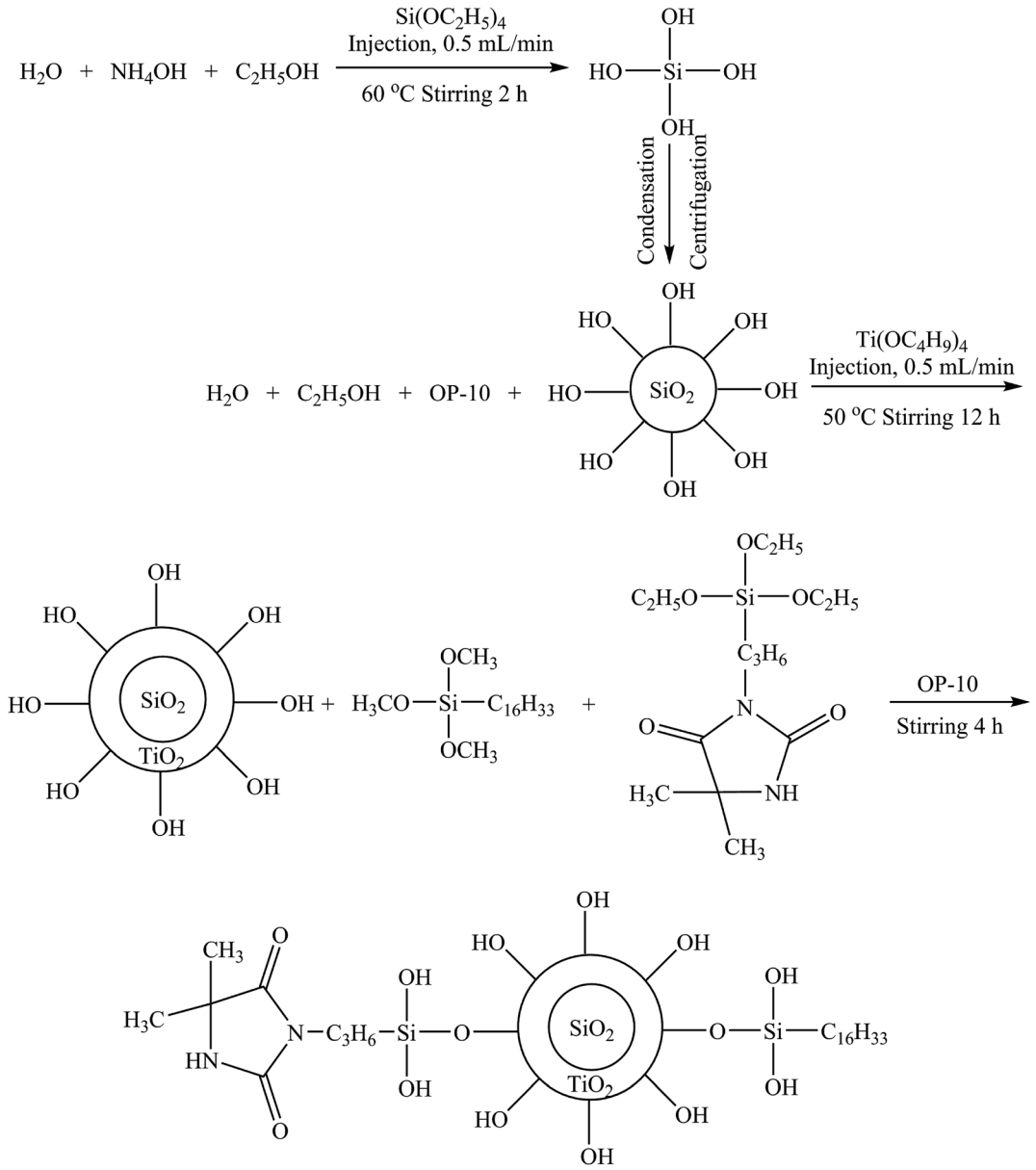

Scheme 1 Synthesis of SiO_2@TiO_2-based core@shell composite nanoparticles.

properties for samples according to the modified AATCC 100-2004 method. In this test, a certain volume of bacterial suspensions (10^6–10^7 CFU) were added to the center between two pieces of fibrous membranes (2.54 × 2.54 cm^2) and the sample assemblies were held in place by putting a sterile weight on top to make sufficient contact between the bacteria and the membranes. After exposure to the bacteria for 5, 10, 30 and 60 min, the membranes were quenched with 5.0 mL sterile 0.02 N sodium thiosulfate solutions to remove oxidative chlorine residuals and vortexed to release bacteria from fibrous membranes to solution. 10-fold serial dilutions of the sterilized solutions were prepared with phosphate buffer (100 mM, pH 7), and each dilution was plated on Trypticase soy agar plate. The agar plates were incubated at 37 °C for 24 h, and the bacterial colony counts were calculated for biocidal efficacy analysis.

3.8 Cell viability test

In vitro biocompatibility of fibrous membranes was tested on rat skin fibroblasts (ATCC CRL-1213) according to International Standard Organization (ISO/EN 10993-5).[44] Rat skin fibroblasts were cultured in a media of Dulbecco's Modified Eagle Medium (DMEM), Fetal Bovine Serum (FBS) and Penstrip (v/v/v, 100 : 10 : 1) at 37 °C under 5% CO_2 atmosphere. After culturing 3 generation of cells, an aliquot of 100 μL cell suspension (~10^4 cells) was seeded in each well of 96-well plates, and, meanwhile, the membranes were immersed into culture medium at 37 °C under 5% CO_2 atmosphere for 24 h to prepare liquid extracts. After 24 h incubation, the culture medium was replaced with liquid extracts. After another 24 h incubation with the extracts, 100 μL of fresh medium and 50 μL of XTT/PMS reagent (v/v, 50 : 1) were replaced to each well and

 This journal is © The Royal Society of Chemistry 2019

Open Access Article. Published on 25 July 2019. Downloaded on 1/9/2025 2:40:26 AM.
This article is licensed under a Creative Commons Attribution-NonCommercial 3.0 Unported Licence.

the plates were incubated dark for another 2–4 h. The absorbance of each well at $OD_{490\ nm}$ was measured with a reference wavelength of $OD_{690\ nm}$ using a microplate reader (Infinity M200 Pro, Tecan). Cells only incubated in culture medium were tested under the same conditions to act as negative controls and data were normalized with this blank control.

3.9 Contact angle measurements

Water contact angle was tested by digital microscope contact angle tester (26700-300, Instrument & Equipment Specialties Inc., USA). 2 μL of distilled water was dropped on the surface of fibrous membranes, and the contact angle was recorded after 1 min for more than 5 times in different positions to calculate the average value for each sample.

3.10 UV light stability test

The chlorine stability of the PHB/PCL–SiO_2@TiO_2–HDTMS/SPH–Cl fibrous membranes under UV light was measured using a model Accelerated Weathering Tester (Q-LAB Company, USA). The PHB/PCL–SiO_2@TiO_2–HDTMS/SPH–Cl fibrous membranes were placed in a UV chamber (type A, 315–400 nm, 0.89 W, 60 °C). After 1, 2, 4, 8, 12 and 24 h of UV light irradiation, the fibrous membranes were removed from the UV chamber and their chlorine contents were measured immediately. The membranes after irradiation for 24 h were rechlorinated and their chlorine contents again determined by titration.

3.11 Storage stability test

The PHB/PCL–SiO_2@TiO_2–HDTMS/SPH–Cl fibrous membranes were placed into self-sealed bags in a dark environment. After a specific time (10, 20, 30, 45 and 60 d), the chlorine contents in the fibrous membranes were calculated by titration method. After 60 days, the fibrous membranes were rechlorinated. The chlorine contents of rechlorinated fibrous membranes were determined.

4 Conclusions

We synthesized SiO_2@TiO_2-based core@shell composite nanoparticles with the average diameter 274.5 ± 16 nm. SEM and FT-IR results showed that the fibrous membranes surfaces were modified with the SiO_2@TiO_2-based core@shell composite nanoparticles. The prepared fibrous membranes had excellent hydrophobicity with an average water contact angle of 144° ± 1° and favorable air permeability. The chlorinated fibrous membranes could inactivate 100% *S. aureus* and *E. coli* O157:H7 within 5 min and 60 min of contact, respectively. The cytotoxicity test demonstrated that the modified fibrous membranes have no cytotoxicity, and the chlorinated fibrous membranes could promote cell growth. The stability tests indicated that the chlorinated fibrous membranes exhibited excellent UVA light stability and superior storage stability. Therefore, the designed multifunctional fibrous membranes may find many suitable applications in the packaging and biomedical materials industry.

Conflicts of interest

There are no conflicts to declare.

Acknowledgements

We would like to thank for the support of the Project of Jiangsu Science and Technological Innovation Team, and the Fundamental Research Funds for the Central Universities (No. JUSRP51722B, No. JUSRP11806), the National First-Class Discipline Program of Light Industry Technology and Engineering (LITE2018-2), and 111 Projects (B17021).

References

1 L. S. Montagna, A. L. Catto, M. M. D. Forte, E. Chiellini, A. Corti, A. Morelli and R. M. C. Santana, *Polym. Degrad. Stab.*, 2015, **120**, 186–192.
2 A. A. Shah, F. Hasan, A. Hameed and S. Ahmed, *Biotechnol. Adv.*, 2008, **26**, 246–265.
3 L. S. Montagna, T. L. D. Montanheiro, A. C. Borges, C. Y. Koga-Ito, A. P. Lemes and M. C. Rezende, *J. Appl. Polym. Sci.*, 2017, **134**, 44234–44242.
4 M. B. Patel, S. A. Patel, A. Ray and R. M. Patel, *J. Appl. Polym. Sci.*, 2003, **89**, 895–900.
5 E. S. Park, H. J. Lee, H. Y. Park, M. N. Kim, K. H. Chung and J. S. Yoon, *J. Appl. Polym. Sci.*, 2001, **80**, 728–736.
6 L. Kou, J. Liang, X. H. Ren, H. B. Kocer, S. D. Worley, R. M. Broughton and T. S. Huang, *Colloids Surf., A*, 2009, **345**, 88–94.
7 E. I. Shishatskaya, T. G. Volova, A. P. Puzyr, O. A. Mogilnaya and S. N. Efremov, *J. Mater. Sci.: Mater. Med.*, 2004, **15**, 719–728.
8 J. M. Lagaron and E. Nunez, *J. Plast. Film Sheeting*, 2012, **28**, 79–89.
9 J. G. Fernandes, D. M. Correia, G. Botelho, J. Padrao, F. Dourado, C. Ribeiro, S. Lanceros-Mendez and V. Sencadas, *Polym. Test.*, 2014, **34**, 64–71.
10 D. Guldiren and S. Aydin, *Mater. Sci. Eng., C*, 2017, **78**, 826–832.
11 T. Uchimaru, S. Tsuzuki, L. Chen and J. Mizukado, *J. Fluorine Chem.*, 2017, **194**, 33–39.
12 M. L. Yin, X. L. Chen, R. Li, D. Huang, X. Y. Fan, X. H. Ren and T. S. Huang, *J. Appl. Polym. Sci.*, 2016, **133**, 44204–44211.
13 X. H. Ren, L. Kou, J. Liang, S. D. Worley, Y. M. Tzou and T. S. Huang, *Cellulose*, 2008, **15**, 593–598.
14 X. H. Ren, L. Kou, H. B. Kocer, C. Y. Zhu, S. D. Worley, R. M. Broughton and T. S. Huang, *Colloids Surf., A*, 2008, **317**, 711–716.
15 R. Li, P. Hu, X. H. Ren, S. D. Worley and T. S. Huang, *Carbohydr. Polym.*, 2013, **92**, 534–539.
16 J. Li, Y. Liu, Z. M. Jiang, K. K. Ma, X. H. Ren and T. S. Huang, *Ind. Eng. Chem. Res.*, 2014, **53**, 13058–13064.
17 H. B. Kocer, S. D. Worley, R. M. Broughton and T. S. Huang, *React. Funct. Polym.*, 2011, **71**, 561–568.
18 I. Cerkez, H. B. Kocer, S. D. Worley, R. M. Broughton and T. S. Huang, *Cellulose*, 2012, **19**, 959–966.

Open Access Article. Published on 25 July 2019. Downloaded on 1/9/2025 2:40:26 AM.
This article is licensed under a Creative Commons Attribution-NonCommercial 3.0 Unported Licence.

19 Y. Liu, Q. H. He, R. Li, D. Huang, X. H. Ren and T. S. Huang, *Fibers Polym.*, 2016, **17**, 2035–2040.
20 A. Nesic, J. Ruzic, M. Gordic, S. Ostojic, D. Micic and A. Onjia, *Composites, Part B*, 2017, **110**, 56–61.
21 M. Nosonovsky and B. Bhushan, *Microelectron. Eng.*, 2007, **84**, 382–386.
22 A. I. Safonov, S. V. Starinskii, V. S. Sulyaeva, N. I. Timoshenko and E. Y. Gatapova, *Tech. Phys. Lett.*, 2017, **43**, 159–161.
23 R. Li, M. M. Sun, Z. M. Jiang, X. H. Ren and T. S. Huang, *Fibers Polym.*, 2014, **15**, 234–240.
24 X. G. Zhang, H. Y. Wang, Z. J. Liu, Y. X. Zhu, S. Q. Wu, C. J. Wang and Y. J. Zhu, *Appl. Surf. Sci.*, 2017, **396**, 1580–1588.
25 F. Kayaci, O. C. O. Umu, T. Tekinay and T. Uyar, *J. Agric. Food Chem.*, 2013, **61**, 3901–3908.
26 X. Y. Fan, Q. Y. Jiang, Z. Sun, G. Li, X. H. Ren, J. Liang and T. S. Huang, *Fibers Polym.*, 2015, **16**, 1751–1758.
27 S. H. Park, S. M. Lee, H. S. Lim, J. T. Han, D. R. Lee, H. S. Shin, Y. J. Jeong, J. Kim and J. H. Cho, *ACS Appl. Mater. Interfaces*, 2010, **2**, 658–662.
28 J. E. Q. Quinsaat, F. A. Nuesch, H. Hofmann and D. M. Opris, *RSC Adv.*, 2013, **3**, 6964–6971.
29 M. Meng, H. W. He, J. Xiao, P. Zhao, J. L. Xie and Z. S. Lu, *J. Colloid Interface Sci.*, 2016, **461**, 369–375.
30 C. R. Li, X. O. Zhang and Z. X. Cao, *Science*, 2005, **310**, 236.
31 J. P. Cook and D. D. Evanoff, *Abstr. Pap. Am. Chem. Soc.*, 2014, 247.
32 X. H. Lin, Y. M. Li, Y. Liu, L. Li, X. H. Ren, Y. Y. Sun and T. S. Huang, *J. Ind. Eng. Chem.*, 2018, **63**, 303–311.
33 H. B. Kocer, A. Akdag, S. D. Worley, O. Acevedo, R. M. Broughton and Y. N. Wu, *ACS Appl. Mater. Interfaces*, 2010, **2**, 2456–2464.
34 V. De Matteis, L. Rizzello, M. P. Di Bello and R. Rinaldi, *J. Nanopart. Res.*, 2017, **19**, 196–210.
35 J. Li, R. Li, J. M. Du, X. H. Ren, S. D. Worley and T. S. Huang, *Cellulose*, 2013, **20**, 2151–2161.
36 Y. Zhao, Y. W. Tang, X. G. Wang and T. Lin, *Appl. Surf. Sci.*, 2010, **256**, 6736–6742.
37 S. Lee, Y. C. Cha, H. J. Hwang, J. W. Moon and I. S. Han, *Mater. Lett.*, 2007, **61**, 3130–3133.
38 C. Chaikeaw and K. Srikulkit, *J. Sol-Gel Sci. Technol.*, 2017, **81**, 774–781.
39 Y. Chen, L. Wang, H. J. Yu, Q. Shi and X. C. Dong, *J. Mater. Sci.*, 2007, **42**, 4018–4024.
40 Y. F. Wang, L. Li, Y. Liu, X. H. Ren and J. Liang, *Mater. Sci. Eng., C*, 2016, **69**, 1075–1080.
41 X. L. Li, Y. Liu, Z. M. Jiang, R. Li, X. H. Ren and T. S. Huang, *Cellulose*, 2015, **22**, 3609–3617.
42 M. F. Richter, B. S. Drown, A. P. Riley, A. Garcia, T. Shirai, R. L. Svec and P. J. Hergenrother, *Nature*, 2017, **545**, 299–304.
43 X. Lin, X. Fan, R. Li, Z. Li, T. Ren, X. Ren and T. S. Huang, *Polym. Adv. Technol.*, 2017, **29**, 481–489.
44 I. 10993-5, International Organization for Standardization Geneve, Switzerland, 2009.
45 R. Li, J. F. Dou, Q. Y. Jiang, J. Li, Z. W. Xie, J. Liang and X. H. Ren, *Chem. Eng. J.*, 2014, **248**, 264–272.
46 X. Y. Fan, X. H. Ren, T. S. Huang and Y. Y. Sun, *RSC Adv.*, 2016, **6**, 42600–42610.
47 Y. Liu, J. Li, L. Li, S. McFarland, X. H. Ren, O. Acevedo and T. S. Huang, *ACS Appl. Mater. Interfaces*, 2016, **8**, 3516–3523.
48 X. H. Ren, A. Akdag, H. B. Kocer, S. D. Worley, R. M. Broughton and T. S. Huang, *Carbohydr. Polym.*, 2009, **78**, 220–226.
49 S. D. Worley, Y. Chen, J. W. Wang and R. Wu, *Surf. Coat. Int., Part B*, 2005, **88**, 93–99.

This journal is © The Royal Society of Chemistry 2019